Size-Exclusion Colloidal Transport in Porous Media—Stochastic Modeling and Experimental Study

Zhenjiang You, Alexander Badalyan, and **Pavel Bedrikovetsky,** University of Adelaide

Summary

Suspension, colloidal, and emulsion flow in rocks with particle size-exclusion may have a strong effect on the reservoir and on the well behavior during fines migration and production, drilling-fluid invasion into oil- or gas-bearing formations, or injection of seawater or produced water. The stochastic microscale equations for size-exclusion colloidal transport in porous media (PM) are derived. The proposed model includes the following new features: It accounts for the accessible flux in the expression for capture rate, it accounts for the increase of inlet concentration caused by the injected particles entering only the accessible area, and it accounts for the dilution of effluent accessible flux in the overall flux of the produced suspension.

Two sets of laboratory tests on short-term injection of monosized suspensions have been carried out in engineered PM. The treatment of the laboratory data for short-term continuous-suspension injection shows good agreement with the modeling results. The proposed model shows a better fit to the experimental data than the previous population-balance model for suspension transport in PM, which validates the proposed modified model.

Introduction

Suspension and emulsion transport in PM is an essential feature of numerous petroleum-production processes (Civan 2007; Ding 2010). Invasion of the drilling fluid into oil- or gas-bearing formations causes well-index reduction; the invasion profile is an important part of the reservoir characterization by well logging (Bailey et al. 2000; Tiab and Donaldson 2004). Injection of poor-quality water, including raw-water injection and produced-water reinjection, may cause significant injectivity damage (Pang and Sharma 1997; Bachman et al. 2003). High-velocity flow of water with a composition different from that of the formation water may lift the reservoir fines; fines migration and capture near production and injection wells may cause a significant well impairment (Sharma and Yortsos 1987c; Khilar and Fogler 1998; Schembre and Kovscek 2005; Civan 2010; Takahashi and Kovscek 2010). Other cases of formation damage resulting from the flow and capture of solid and liquid particles in oil and gas reservoirs include asphaltene and paraffin precipitation, production of foamy oils, flow of foams, and invasion of completion fluids. Industrial filtering, propagation of bacteria and viruses in aquifers, disposal of industrial wastes, and artesian-well exploitation are some examples of the numerous nonpetroleum applications of suspension and emulsion transport in PM (Torkzaban et al. 2010; Bradford et al. 2011; Chatterjee et al. 2011).

The rock alteration in the preceding processes is a result of particle capture by the matrix, which leads to permeability damage. Such capture is caused by size exclusion of large particles, particle/grain attachment, gravity segregation, particle diffusion into dead-end pores, and bridging (Nabzar et al. 1996; Chauveteau et al. 1998; Rousseau et al. 2008; Saraf et al. 2010). The straining mechanism, in which large particles become stuck in thin pores (size-exclusion capture), often occurs in formation-damage processes.

Original SPE manuscript received for review 1 December 2011. Revised manuscript received for review 15 April 2012. Paper (SPE 162941) peer approved 30 May 2012.

The reliable mathematical modeling of the preceding processes is aimed at strategy development for injected-water treatment, particle sizing in drilling and completion fluids, design of injected-water filtering, and gravel sizing in frac-pack and gravel-pack well completions. At present, the suspension and emulsion transport in natural rocks on the microscale is modeled using population-balance models (Sharma and Yortsos 1987a,b; Bedrikovetsky 2008), random-walk equations (Cortis and Berkowitz 2004; Shapiro and Bedrikovetsky 2008, 2010), the mean-field model (Lin et al. 2009), and numerical network models (Nabzar et al. 1996; Chauveteau et al. 1998; Bradford et al. 2009). Upscaling or averaging of microscale models results in different versions of the so-called classical deep-bed filtration models (Herzig et al. 1970; Tufenkji 2007; Mojarad and Settari 2007, 2008; Bedrikovetsky 2008; Lin et al. 2009; Massoudieh and Ginn 2010). The extensive literature is devoted to laboratory validation of the models. Yet, to meet the capture conditions for environmental- and chemical-engineering processes, the laboratory studies have concentrated mostly on attachment, sedimentation, and diffusive mechanisms. Several experimental studies include size-exclusion capture, but never as a dominant capture process (Mays and Hunt 2005; Chupin et al. 2008; Bradford et al. 2009; Zhou et al. 2009; Noubactep and Caré 2010; Richards and Neretnieks 2010; Gitis et al. 2010). To the best of our knowledge, an experimental validation of size-exclusion deep-bed filtration models is unavailable in the literature.

In the present work, the size-exclusion population-balance model for suspension transport in rocks has been modified by taking into account the porous space accessibility and fractional flow in inlet and effluent boundary conditions, and also in the expression for the particle-capture rate. The laboratory tests on size-exclusion deep-bed filtration have been carried out in the engineered PM. Good agreement between the modeling prediction and the laboratory data validates the proposed model.

The structure of this paper is as follows. First, the stochastic micromodel for suspension flow in PM, accounting for straining, is presented, followed by an analytical solution to the case of low-retention filtration. Then, the detailed description of experimental procedures is given. Afterward, we check the fulfillment of the low-retention assumption under the test conditions and present the results of the data treatment by the low-retention analytical model. The comparison between the modified and previous models is performed by comparing modeling results with experimental data. The following discussions include the model limitations and methods to improve the experimental techniques. The assumptions state the differences between the modified and previous models and the results of the experimental model validation. Then, the latest improvements to the experimental procedure are highlighted. Afterward, the treatment of experimental data with the analytical model is presented and analyzed. Finally, some discussions and conclusions conclude the paper.

Microscale Modeling for Particle Straining

The stochastic modeling of suspension flow in PM, accounting for straining particle capture, is established in this section. The medium is represented by the model of triangular parallel capillaries alternated with mixing chambers. The analytical model for low-retention filtration is derived, and the steady-state solution is obtained.

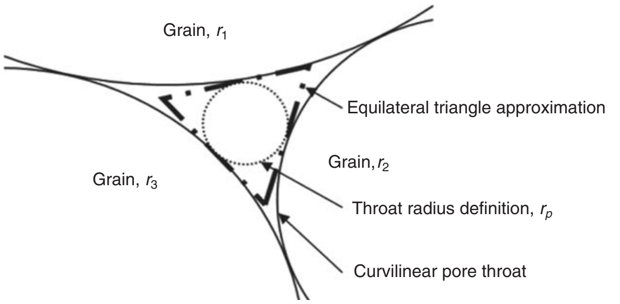

Fig. 1—The cross section of a pore throat formed by three tangent spherical grains.

The main assumptions include incompressibility of rock and particles, 1:1 ratio of plugged pores to strained particles, repulsion between particles and the matrix, and size exclusion as the only particle-capture mechanism. Thus, the particles are considered to be solid.

Basic Parameters and Functions. In this subsection, we define the essential parameters and functions that form the basis of the proposed stochastic micromodel.

Packed spherical grains form the engineered PM. **Fig. 1** illustrates the cross section of a pore throat created by neighboring tangent grains. The radius of the maximum inscribed sphere r_p is introduced to characterize the pore size. A pore of size r_p will allow a particle of size r_s to enter, only if the following condition is satisfied:

$$r_s < r_p. \quad (1)$$

Accordingly, this type of particle-retention mechanism is termed as particle straining or size exclusion.

For simplicity, most researchers involved in microscopic-scale modeling have adopted the shape of a pore throat as being circular (Sharma and Yortsos 1987a,b,c; Bedrikovetsky 2008). However, Fig. 1 shows clearly that the pore-throat shape is actually a curvilinear triangle. In this study, we take the equilateral triangle having the maximum inscribed pore-throat radius to better approximate the curvilinear pore throat.

As shown in **Figs. 2a and 2b,** the model represents a PM as a bundle of parallel capillaries with concentration distribution $H(r_p,x,t)$, alternated by a series of chambers with an interval of l, in which suspended particles are mixed completely and redistributed (Bedrikovetsky 2008). The geometrical model of a porous space as a set of parallel capillaries intercalated by mixing is

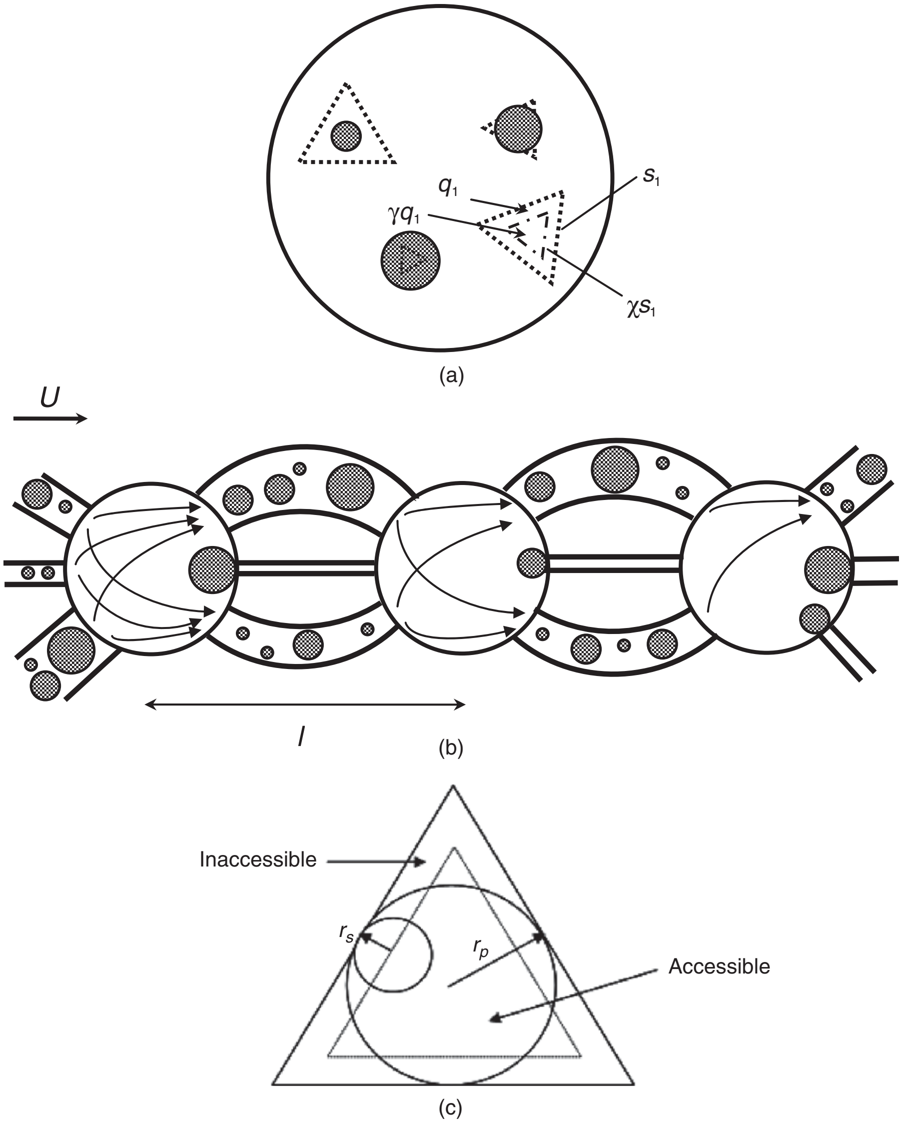

Fig. 2—Schematic of size-exclusion suspension flow in PM represented by the model of parallel capillaries with mixing chambers: (a) size-distributed capillaries with triangular cross section; (b) flow through capillaries into mixing chambers; (c) accessible and inaccessible fractions of pore cross section.

determined fully by the pore-size distribution (PSD) and the interchamber distance. A suspended particle may only be transported through a pore with a throat size that is larger than the particle. After arrival to the chamber from the pore outlets, particles with different sizes are mixed completely and transported to the entrances of the next bundle of pores. The probability of particles reaching the pores with different sizes is proportional to the carrier water fluxes in those pores. Whether a particle is captured by a pore or not is determined solely by the condition that the particle size is larger or smaller than the pore size. Therefore, all the suspended particles are sieved effectively according to their sizes at the entrance of each capillary bundle. A dimensionless term, the jamming ratio j, is defined as the ratio of particle size to pore size:

$$j = \frac{r_s}{r_p}. \quad (2)$$

The total concentration of pores of all sizes, $h(x,t)$, is defined as the total number of pores per unit surface area at a distance x and time t:

$$h(x,t) = \int_0^\infty H(r_p,x,t)\mathrm{d}r_p, \quad (3)$$

where $H(r_p,x,t)\mathrm{d}r_p$ is the concentration of pores with sizes between r_p and $r_p + \mathrm{d}r_p$.

In a similar manner, the overall concentration of suspended particles in PM, $c(x,t)$, is defined as the total number of all suspended particles per unit volume of suspension at a certain distance x and time t, resulting from the integration of concentration of these particles in terms of r_s:

$$c(x,t) = \int_0^\infty C(r_s,x,t)\mathrm{d}r_s, \quad (4)$$

where $C(r_s,x,t)$ is the particle-concentration distribution function. The concentration distribution of retained particles, $\Sigma(r_s,x,t)$, is defined as the number of retained particles, $\Sigma(r_s,x,t)\mathrm{d}r_s$, with radii between r_s and $r_s + \mathrm{d}r_s$. The total concentration of retained particles, $\sigma(x,t)$, is obtained by

$$\sigma(x,t) = \int_0^\infty \Sigma(r_s,x,t)\mathrm{d}r_s. \quad (5)$$

Because both the particle size and the pore size affect the particle capture, the retained particle concentration can also be distributed according to r_p. Therefore, we introduce $\underline{\Sigma}(r_p,r_s,x,t)$ as the distribution of retained particle concentration over the pore and particle radii:

$$\Sigma(r_s,x,t) = \int_0^\infty \underline{\Sigma}(r_p,r_s,x,t)\mathrm{d}r_p. \quad (6)$$

The triangular cross-sectional area of a single pore with size r_p is

$$s_1(r_p) = 3\sqrt{3}r_p^2. \quad (7)$$

The accessibility of pore space to a particle with particular size is restricted by the particle radius. Fig. 2c illustrates the accessible and inaccessible areas in a single pore. The ratio of the accessible fraction to the total cross-sectional area is defined as the accessibility factor $\chi(j)$:

$$\chi(j) = \begin{cases} (1-j)^2, & j<1 \\ 0, & j>1 \end{cases}, \quad (8)$$

which is the result of calculating the ratio $3\sqrt{3}(r_p - r_s)^2/s_1(r_p)$ with Eq. 7.

The accessible porosity is obtained from the total accessible pore cross-sectional area per unit of the PM cross section:

$$\phi_a[H,r_s] = \int_{r_s}^\infty s_1(r_p)\chi(j)H(r_p,x,t)\mathrm{d}r_p. \quad (9)$$

The parentheses are used for the functions of scalar variables, and the square brackets are used for functional of functions.

The accessible and inaccessible flow fractions, f_a and f_{ns}, respectively, are defined as

$$f_a = \frac{U_a}{U} = \frac{\int_{r_s}^\infty k_1(r_p)\gamma(j)H(r_p,x,t)\mathrm{d}r_p}{\int_0^\infty k_1(r_p)H(r_p,x,t)\mathrm{d}r_p} \quad (10)$$

and

$$f_{ns} = \frac{U_{ns}}{U} = \frac{\int_0^{r_s} k_1(r_p)H(r_p,x,t)\mathrm{d}r_p}{\int_0^\infty k_1(r_p)H(r_p,x,t)\mathrm{d}r_p}, \quad (11)$$

where $k_1(r_p)$ is the hydraulic conductance through a single pore and $\gamma(j)$ is the flux-reduction factor through a single pore.

Let us define the flux reduction factor γ as the ratio of the flux by means of the accessible area of a single triangular pore to the total flux (Fig. 2c). The explicit formula for conductance of the triangular pore follows the explicit formula for steady-state flow of the viscous fluid through a triangular pore (Poiseuille flow); see Bird et al. (2007).

$$k_1(r_p) = \frac{9\sqrt{3}}{20}r_p^4. \quad (12)$$

The flux reduction factor is calculated from the Poiseuille flow formula as a ratio of the conductance of the accessible area to the overall pore conductance:

$$\gamma(j) = \begin{cases} (1-j)^2\left(1+2j-\frac{1}{3}j^2-\frac{4}{9}j^3\right), & j<1 \\ 0, & j>1 \end{cases}. \quad (13)$$

Governing Equations of Suspension Transport in PM. In this subsection, the governing equations of suspension transport in PM with derivations are presented briefly. For further details, refer to earlier publications by Sharma and Yortsos (1987a,b) and Bedrikovetsky (2008).

The population-balance equation for colloidal particles in PM has the following form:

$$\frac{\partial}{\partial t}\{\phi_a[H,r_s]C(r_s,x,t)\} + U\frac{\partial}{\partial x}\{C(r_s,x,t)f_a[H,r_s]\} = -\frac{\partial}{\partial t}\Sigma(r_s,x,t), \quad (14)$$

where the total flux U is independent of the coordinate x because of the incompressibility of the particulate suspension.

In the following, we derive the equations for kinetics of the particle capture and consequent pore plugging. The suspended particle concentration in the accessible fraction is $f_aC(r_s,x,t)$. The assumption of complete mixing between capillary bundles indicates that colloidal particles are presented randomly to a pore throat, and there exists no preference for a colloidal particle to a particular throat. Therefore, the number of r_s particles arriving from the chambers to pores with size r_p by the flow per unit volume during the time interval Δt is

$$\frac{1}{l}q_1(r_p)H(r_p,x,t)C(r_s,x,t)f_a[H,r_s]\Delta t, \quad (15)$$

where q_1 is the flow rate in a single pore. Under the particle/grain repulsion condition, particles are not captured in the inaccessible portion of larger pores. Instead, they are redirected and enter the accessible pore space. Thus, the suspended particles are captured by smaller pores only. The probability for a particle to be captured is equal to the flow fraction by means of small inaccessible pores, f_{ns}.

TABLE 1—MEAN RADIUS $\langle r_s \rangle$ OF COLLOIDAL PARTICLES FOR PM1

Type of Particles	$\langle r_s \rangle$, μm
1	0.886
2	1.032
3	1.568
4	2.179
5	3.165

The retention rate of particles with size r_s being captured by pores with size $r_p (r_p < r_s)$ is equal to the overall particle flux from the chambers into these small pores:

$$\frac{\partial \underline{\Sigma}(r_p, r_s, x, t)}{\partial t} = \frac{1}{l} q_1(r_p) H(r_p, x, t) C(r_s, x, t) f_a[H, r_s]. \quad \ldots (16)$$

Integration of Eq. 16 into r_p for all smaller pores leads to the equation for the particle-retention rate with size r_s:

$$\frac{\partial \Sigma(r_s, x, t)}{\partial t} = \frac{1}{l} UC(r_s, x, t) f_a[H, r_s] f_{ns}[H, r_s]. \quad \ldots\ldots\ldots (17)$$

The rate of pore plugging with size r_p because of particle capture is equal to the overall flux of larger particles flowing into r_p pores from chambers:

$$\frac{\partial H(r_p, x, t)}{\partial t} = -\frac{k_1(r_p)}{k} UH(r_p, x, t) \int_{r_p}^{\infty} C(r_s, x, t) f_a[H, r_s] \mathrm{d}r_s, \quad \ldots\ldots\ldots\ldots\ldots\ldots (18)$$

which results from the assumption that one retained particle plugs one pore.

Substituting the retention-rate equation (Eq. 17) into the population-balance equation (Eq. 14) yields

$$\frac{\partial}{\partial t}\{\phi_a[H, r_s] C(r_s, x, t)\} + U \frac{\partial}{\partial x}\{C(r_s, x, t) f_a[H, r_s]\} = -\frac{1}{l} UC(r_s, x, t) f_a[H, r_s] f_{ns}[H, r_s]. \quad \ldots\ldots\ldots (19)$$

The system of two equations (Eqs. 18 and 19) for two unknowns describes the size-exclusion deep-bed filtration process. The initial conditions for the clean bed include zero suspension concentration and initial uniform PSD for pores:

$$t = 0\colon\ C(r_s, x, 0) = 0,\ H(r_p, x, 0) = H_0(r_p). \quad \ldots\ldots \quad (20)$$

The boundary condition at the inlet states that the suspension flux entering larger pores with the injected concentration is equal to the suspension flux transported by water in accessible pore space:

$$x = 0\colon\ C^0(r_s, t)\{f_a[H, r_s] + f_{nl}[H, r_s]\} U = C(r_s, 0, t) f_a[H, r_s] U. \quad \ldots\ldots\ldots\ldots\ldots (21)$$

Eq. 21 indicates that the post-inlet concentration exceeds the injected-particle concentration.

Analytical Solution for Low-Retention Filtration. Low-retention filtration takes place at short-term injection, at injection of diluted suspension, or when there is a small filtration coefficient (small particle size). In all these cases, the retained particle concentration is negligible compared with the vacant-pore concentration. Hence, the pore concentration remains intact during this process. Eq. 19 is simplified to an ordinary-differential equation for steady state:

$$U \frac{\mathrm{d}}{\mathrm{d}x}\{C(r_s, x) f_a[H, r_s]\} = -\frac{1}{l} UC(r_s, x) f_a[H, r_s] f_{ns}[H, r_s]. \quad \ldots\ldots\ldots\ldots\ldots\ldots (22)$$

The fractional-flow functions in Eq. 22 depend only on particle size because of constant PSD during injection [i.e., $H(r_p,x,t) = H_0(r_p)$]. Therefore, Eq. 22 can be solved independently for each particle size, which implies that particles with different sizes percolate independently and deposit as a group of monodisperse suspensions. Hence, the governing equation (Eq. 22) becomes

$$\frac{\mathrm{d}C(r_s, x)}{\mathrm{d}x} = -\frac{1}{l} f_{ns}(r_s) C(r_s, x), \quad \ldots\ldots\ldots\ldots\ldots (23)$$

with the boundary condition

$$C(r_s, 0) = \frac{C^0(r_s)[f_a(r_s) + f_{nl}(r_s)]}{f_a(r_s)}. \quad \ldots\ldots\ldots\ldots\ldots (24)$$

The solution to this ordinary differential equation is named the preoutlet particle concentration:

$$C(r_s, x) = \frac{C^0(r_s)[f_a(r_s) + f_{nl}(r_s)]}{f_a(r_s)} \exp\left[-f_{ns}(r_s)\frac{x}{l}\right]. \quad \ldots\ldots (25)$$

We define $C^L(r_s)$ as the outlet particle concentration [also called the breakthrough or effluent concentration (they are equivalent in this work)], which is measured from the collected sample at the outlet. Because the preoutlet suspension flux is diluted in the overall water flux after passing the core outlet, we have

$$C(r_s, L) f_a(r_s) U = C^L(r_s) U. \quad \ldots\ldots\ldots\ldots\ldots (26)$$

Eqs. 25 and 26 lead to the relationship between the measured particle concentrations at the outlet and inlet:

$$C^L(r_s) = C^0(r_s)[f_a(r_s) + f_{nl}(r_s)] \exp\left[-f_{ns}(r_s)\frac{L}{l}\right]. \quad \ldots\ldots (27)$$

As shown in Eq. 27, the larger particle size results in the higher flow fraction by means of inaccessible small pores (f_{ns}), the lower flow fraction by means of large pores ($f_a + f_{nl}$), and, finally, the lower outlet concentration C^L. When the particle size reaches the maximum pore size, the outlet concentration vanishes because the flow fraction by means of large pores drops to zero.

Experimental Study on Size-Exclusion Suspension Transport

In this section, the experimental conditions of particle/particle and particle/grain repulsion, leading to the absence of particle retention by attachment to the porous matrix, are adopted from a previous study (Chalk et al. 2011). For a given grain and colloid material, the repulsion conditions can be achieved by regulating water pH and salinity (Nabzar et al. 1996; Takahashi and Kovscek 2010). These conditions are then implemented during suspension injection through the column packed with an engineered PM.

Materials. ***Colloidal Suspensions.*** Chemistry of colloidal suspension is very important when studying particulate flow through PM. Variation of salinity and pH in colloidal suspension affects the particle capture/release by PM significantly. In the present study, colloidal particle capture caused by exclusive straining at pore throats is investigated. Chemical compositions of water, grain, and particle coatings provide unfavorable experimental conditions for the particle/particle and particle/grain attraction, so there is no deposition and formation of retained particle structures on the PM skeleton.

Spherical colloidal polystyrene latex particles (Polysciences Inc., Warrington, Pennsylvania, USA) are covered with carboxyl functional groups (R-COOH), giving them the net negative charge that results in mutual particle repulsion. This charge not only prevents particles from coagulation, but results in repulsion with glass beads (engineered PM) because of the reduction of electrostatic attraction forces (see the next subsection). **Tables 1 and 2** list the sizes of the colloidal particles used in the present study. Earlier experiments (Chalk et al. 2011), with a single layer of

TABLE 2—MEAN RADIUS $\langle r_s \rangle$ OF COLLOIDAL PARTICLES FOR PM2

Type of Particles	$\langle r_s \rangle$, μm
1	1.568
2	2.179
3	3.165
4	4.538

glass beads, determined the optimum conditions leading to the repulsion between particles and glass beads and, therefore, to colloidal particle capture because of pure straining at pore throats—zero salinity of water and alkaline nature of colloidal suspension of pH ≈ 10.

The total number of colloidal particles in suspension is chosen so as to reduce the competition between particles entering a pore. In the present experiments, particle concentrations vary from 0.5 to 2.0 ppm.

Engineered PM. The porous column was designed to reproduce the conditions of sandstone reservoirs. Silica (SiO_2) is the major component of sandstones; therefore, spherical glass beads (Ballotini Bead, Potters Industries Pty. Ltd., Australia) have been chosen as engineered PM for the current experimental program. These beads have the following chemical composition by weight: 72.0% SiO_2, 15.0% Na_2O, 7.0% CaO, 4.2% MgO, 0.4% Fe_2O_3, and 0.3% Al_2O_3.

In alkaline solutions with pH of approximately 11, metal oxides presented on the surface of glass beads are charged negatively, thus giving negativity to the net surface charge of glass beads (Kuznar and Elimelech 2007). According to the Derjaguin, Landau, Verwey, and Overbeek (DLVO) theory (Landau and Lifshitz 1980; Tufenkji and Elimelech 2004, 2005), carboxyl-coated latex colloidal particles and glass beads in such alkaline suspensions repulse each other because both have surface-negative charges, resulting in particle/grain repulsion and particle straining as the only mechanism of particle capture.

Reusage of glass beads after contact with colloidal suspensions can reduce preparation time significantly for the next experiments. We observed, however, that after 17 washes with demonized ultrapure MilliQ water (resistivity of 18 MΩ×cm at 25°C) at pH ≈ 10 (one wash is equivalent to 1 L of MilliQ water per 150 g of glass beads), colloids were still present in MilliQ water supernatant in appreciable amounts because only approximately 83% of the particles were removed. Therefore, to improve the reliability and repeatability of experimental data, freshly prepared and washed glass beads were used for each test.

The manufacturer supplied glass beads with radius r_g ranging from 15 to 62.5 μm. These beads were sieved using stainless steel sieves (Callout 1 in **Fig. 3a**) with apertures of 30 and 63 μm, giving the range of bead-particle radius from 15 to 31.5 μm. Glass-bead sieving was carried out in an ultrasonic bath (Callout 2), resulting in the following improvements compared with those from the previous work (Chalk et al. 2011): time of sieving was reduced by 4 times and a higher yield in sieved glass beads and a more efficient usage of glass beads were achieved. The determination of size distribution of thus prepared glass beads was carried out using Malvern Mastersizer 2000 Particle Counter (Malvern Instruments Limited, Worcestershire, UK). Because the results of particle-size distribution using manual sieving and ultrasound bath are almost identical, the latter procedure is preferred over the former because of the advantages mentioned in the preceding.

Before the flow experiments, glass beads were washed carefully with *n*-hexane, acetone, MilliQ water, and 0.5M HCl to adjust the pH of MilliQ supernatant to approximately 7–7.5.

Experimental Setup and Procedure. The procedure for the challenging coreflood testing is illustrated in Fig. 3a, and a photograph of the set of devices is found in Fig. 3b. Detailed description of the experimental method for particle retention caused by pure straining in engineered PM was presented earlier (Chalk et al. 2011). In the following, we discuss the major components of the setup and experimental procedure, together with recently introduced improvements.

The flow through a plastic column (Callout 3 in Fig. 3a and Chalk et al. 2011) was modified by reducing inlet and outlet dead volumes to 14.831 and 9.032 cm^3, respectively. Glass beads (Callout 4) were packed in this column at wet conditions with a theoretical porosity of 39.6%. Sonification of wetted glass beads in the column resulted in a more homogeneous packing. Every effort was made to prevent the ingress of air into the packed column, which can alter particle flow/capture significantly through an engineered PM.

A modified NE-100 dual-pump/syringe system (Callout 5; New Era Pump Systems Inc., Farmingdale, NY, USA) provided pulseless delivery of colloidal suspension (Callout 6) through the packed column by means of a system of nonreturn valves (Callouts 7 through 10 in Fig. 3a). This system can operate unattended for several days, which is an improvement from the previous design (Chalk et al. 2011). The volume of plastic syringes used was 60 mL, with an internal diameter of 29.15 mm. Colloidal suspension through a packed column was delivered with a volumetric flow rate of 2 mL/min, equivalent to an interstitial velocity of 5×10^{-5} m/s.

Colloidal suspensions were collected in sampling vials (Callout 11) at predetermined time intervals after passing through the packed column. Masses of suspension samples were measured by an analytical balance (Callout 12; KERN EW 420-3NM, Inscale Ltd., Bucks, UK) with an accuracy of ±0.005 g, and sample volumes were determined by means of density of colloidal suspensions. Concentrations of initial colloidal suspension and column outlet streams were determined by a PAMAS S4031 GO portable particle counter (Callout 13; PAMAS GmbH, Salzuflen, Germany). Although the manufacturer of the PAMAS particle counter did not provide the value of accuracy in particle-number counting across various particle-size distributions, we have determined the repeatability in determination of concentrations of all particles listed in Table 1 from 10 consecutive measurements of the same colloidal suspension. The obtained values of the standard deviation varied from 0.46 to 2.89%, which can be regarded as the inherent precision of the PAMAS particle counter because it is a component of precision and accuracy according to National Institute of Standards and Technology guidelines (Taylor and Kuyatt 1994). Because the particle counter delivers results of particle number over the chosen size-distribution range, in all our consecutive calculations, we used values of colloidal particle radii calculated as weighted mean values, which are more representative than a mean value supplied by the colloidal particle manufacturer. After particle counting, suspensions were filtered through a 0.45-μm filter (Callout 14) and disposed of according to the regulations of the Australian Environmental Protection Authority.

Because the value of precision for the data delivered by the PAMAS particle counter is known, we have used this value as an indicator to determine if the concentration of the outlet colloidal solution was stabilized: If concentrations of the two consecutive effluent samples differ from each other by the value of less than the inherent precision of the PAMAS particle counter for that particle size, then the flow-through experiment stops; otherwise, it continues.

Colloid concentrations can be measured by online ultraviolet-visible (UV-VIS) spectrophotometers or combined particle counters/particle sizers. The application of spectrophotometers translates to the collection of a significant amount of colloid-concentration data, which is limited only by the properties of the data-acquisition system. Although the number of experimental points increases in this case, most of them are redundant because their availability does not improve the accuracy of the consecutive calculations. Spectrophotometers should be calibrated before concentration measurements. This is achieved through the preparation of several calibrating solutions involving dilutions of a standard colloidal suspension supplied by a manufacturer. The manufacturer

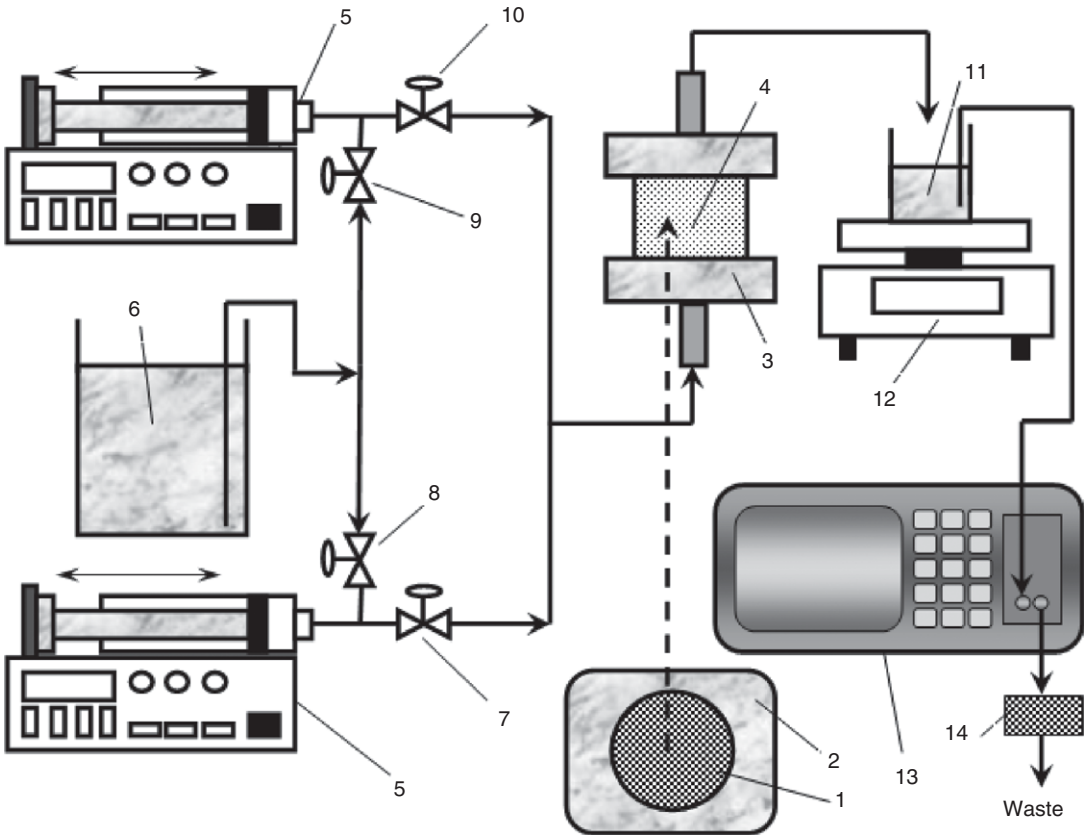

(a)

(b)

Fig. 3—Experimental setup of size-exclusion suspension transport in PM: (a) schematic and (b) photograph.

measures concentration of the standard colloidal suspension using a particle counter/particle sizer. Therefore, uncertainty of the concentration of the standard colloidal suspension depends on the accuracy of such an instrument. Each dilution introduces additional uncertainty into concentration values, the former being dependent on the accuracy of the volumetric device (such as micro- or millipipettes) and on the skills of the operator. Moreover, each spectrophotometer has its own accuracy. Thus, colloidal-concentration value delivered by a spectrophotometer incorporates uncertainties of a particle sizer because of dilution and of a spectrophotometer.

In our approach, the application of the PAMAS particle counter/particle sizer with a carefully established sampling procedure (e.g., number of samples, sampling time intervals, sampling volumes, measuring masses of effluent samples) resulted in the collection of fewer experimental data that were, however, sufficient for the accurate evaluation of the breakthrough curves. Moreover, experimental uncertainties of initial and effluent colloidal-suspension concentrations are determined only by the uncertainty of the PAMAS particle counter, and, therefore, are more accurate than those delivered by UV-VIS spectrophotometer.

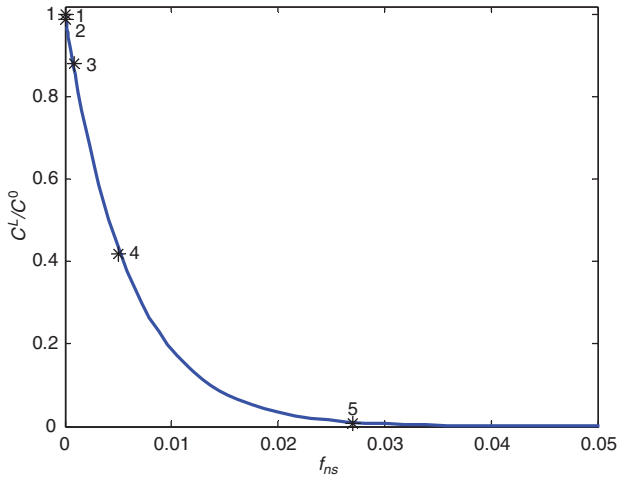

Fig. 4—Effect of fractional flow by means of small pores (f_{ns}) on normalized breakthrough concentration.

Data Analysis for the Laboratory Tests and Modeling Results

In this section, we examine whether the condition of low-retention filtration leading to a simple analytical solution (Eq. 27) is satisfied during the laboratory tests. Subsequently, the results obtained from the suspension injection tests are treated by the proposed analytical model.

Validation of the Low-Retention Assumption. The low-retention assumption of the analytical model (see Analytical Solution for Low-Retention Filtration subsection) is valid,if the vacant-pore concentration is much higher than the concentration of retained particles (i.e., the variation of PSD during particle straining in the PM is negligible). This occurs when

$$\sigma(x,t) \ll h(x,t). \quad \ldots\ldots\ldots\ldots\ldots\ldots\ldots\ldots\ldots\ldots (28)$$

In the case of the performed test, the concentration of vacant pores is $h = pN_p/V$, where N_p is the number of pores, V is the volume of the column, and p is the fraction of vacant pores. The number of packed grains is $N_g = (1-\phi)V/(4\pi r_g^3/3)$, where ϕ is the porosity. For an assumed close and dense grain packing (rhombohedral) in the column, each pore is formed by four grains and each grain is surrounded by eight pores. Hence, $N_p = 2N_g$:

$$N_p = (1-\phi)V/(2\pi r_g^3/3). \quad \ldots\ldots\ldots\ldots\ldots\ldots\ldots\ldots (29)$$

The suspended concentration is smaller than the injected one $c(x,t) < c^0$; the retained particle concentration is limited by $\sigma(x,t) = \lambda c(x,t)Ut \le \lambda c^0 Ut$. Let us define the dimensionless time as $t_D = tU/\phi L$, calculated in pore volumes of injected suspension. The injected concentration c^0 measured in the number of particles per volume of suspension (number concentration) is equivalent to the volumetric concentration measured in ppm divided by the particle volume, $(4\times 10^6 \pi r_s^3/3)$. From Eqs. 28 and 29, the following condition is derived:

$$\frac{\lambda c^0 t_D L\phi}{2\times 10^6 \cdot p(1-\phi)}\left(\frac{r_g}{r_s}\right)^3 \ll 1. \quad \ldots\ldots\ldots\ldots\ldots\ldots (30)$$

It is worth noting that the product $\lambda c^0 t_D$ in the numerator of Eq. 30 indicates that the low-retention case corresponds to one of the following: low injected concentration, short injection time, or small filtration coefficient.

The typical values of the parameters in our experiment are $c^0 = 2$ ppm, $\phi = 0.4$, the measured particle size $r_s = 3.165$ μm, the grain size $r_g = 40$ μm, the fraction of thinner pores $p = 0.3$, and $t_D = 5$ pore volumes injected (PVI), which result in the value 0.017 (the left-hand side of Eq. 30). So, the low-retention condition (Eq. 30) is fulfilled.

Experimental-Data Treatment. The analytical model (Eq. 27) can be applied to calculate the recovered breakthrough concentrations for particles with different sizes injected into the porous column:

$$\frac{C^L(r_s)}{C^0(r_s)} = [1-f_{ns}(r_s)]\exp\left[-f_{ns}(r_s)\frac{L}{l}\right]. \quad \ldots\ldots\ldots\ldots (31)$$

Here, the equivalent term $1-f_{ns}$ substitutes the fractional flux by means of large pores $f_a + f_{nl}$.

From the experiment, the inlet and outlet concentrations $C^0(r_{si})$ and $C^L(r_{si})$, respectively, are measured for each test (here, $i = 1, 2, \ldots, n$). The pore sizes obey the log-normal distribution with mean pore radius $\langle r_p\rangle$ and standard deviation σ_o. The fractional-flow function f_{ns} is calculated using Eq. 11, and then the outlet concentration can be obtained from the model (Eq. 31). Finally, n tests result in the system of n transcendental equations for three unknowns—mean pore radius, standard deviation, and dimensionless interchamber distance. The least-squares method is applied to find the solution by minimizing the total quadratic deviation between the experimental data and those predicted by the model:

$$R = \min_{\langle r_p\rangle,\sigma_0,l/L} \sum_{i=1}^{n}\left\{[1-f_{ns}(r_{si})]\exp\left[-f_{ns}(r_{si})\frac{L}{l}\right] - \frac{C^L(r_{si})}{C^0(r_{si})}\right\}^2, \quad \ldots\ldots\ldots\ldots\ldots (32)$$

where R is the value of the residual.

For PM1, with glass beads ranging in size from approximately 15 to 31.5 μm, the optimized mean pore size is 3.13 μm, the standard deviation is 2.06 μm, and the interchamber distance is 0.36 mm. For PM2, with glass beads ranging in size from approximately 15 to 62.5 μm, the mean pore size is 5.39 μm, the standard deviation is 3.84 μm, and the interchamber distance is 0.06 mm. The results are shown in **Figs. 4 and 5** for PM1 and **Fig. 6** for PM2.

The relationship between the breakthrough concentration and inaccessible flow fraction is shown in Fig. 4, in which the continuous curve is obtained from the analytical model (Eq. 31) and the points represent the experimental data. The breakthrough concentration decreases dramatically with the fractional flux (f_{ns}) because the increase in particle size leads to the larger flow fraction by means of inaccessible small pores, which raises the particle-capture rate significantly and lowers the breakthrough concentration.

Fig. 5a shows the breakthrough curves of PM1 from the injection of monosized particles with the radii listed in Table 1. The stabilized outlet concentrations agree well with the model-predicted values for particles with different sizes. In Fig. 5b, the normalized outlet concentration vs. the jamming ratio is presented. The stabilized values of breakthrough concentrations in all tests are adopted as C^L values. As shown in Fig. 5b, the five laboratory-test data points match very well with the modeling curve, as obtained from Eq. 31.

The breakthrough curves for PM2 from the injection of monosized particles (Table 2) are shown in Fig. 6a. For the four different sized particles, the stabilized outlet concentrations from the experiments are in agreement with those from the model calculation. The normalized outlet concentration vs. jamming ratio is presented in Fig. 6b. It is observed that the four laboratory-test data points match very well with the curve obtained from the model (Eq. 31).

A sensitivity analysis for the three parameters in the model was performed, and the results are shown in **Figs. 7 through 9** and **Table 3.** Fig. 7 illustrates the sensitivity of the outlet concentration to the mean pore radius $\langle r_p\rangle$. Increase of $\langle r_p\rangle$ leads to a lower jamming ratio, with the same particle size and a lower particle concentration, C^L/C^0. In Fig. 8, the variation of standard

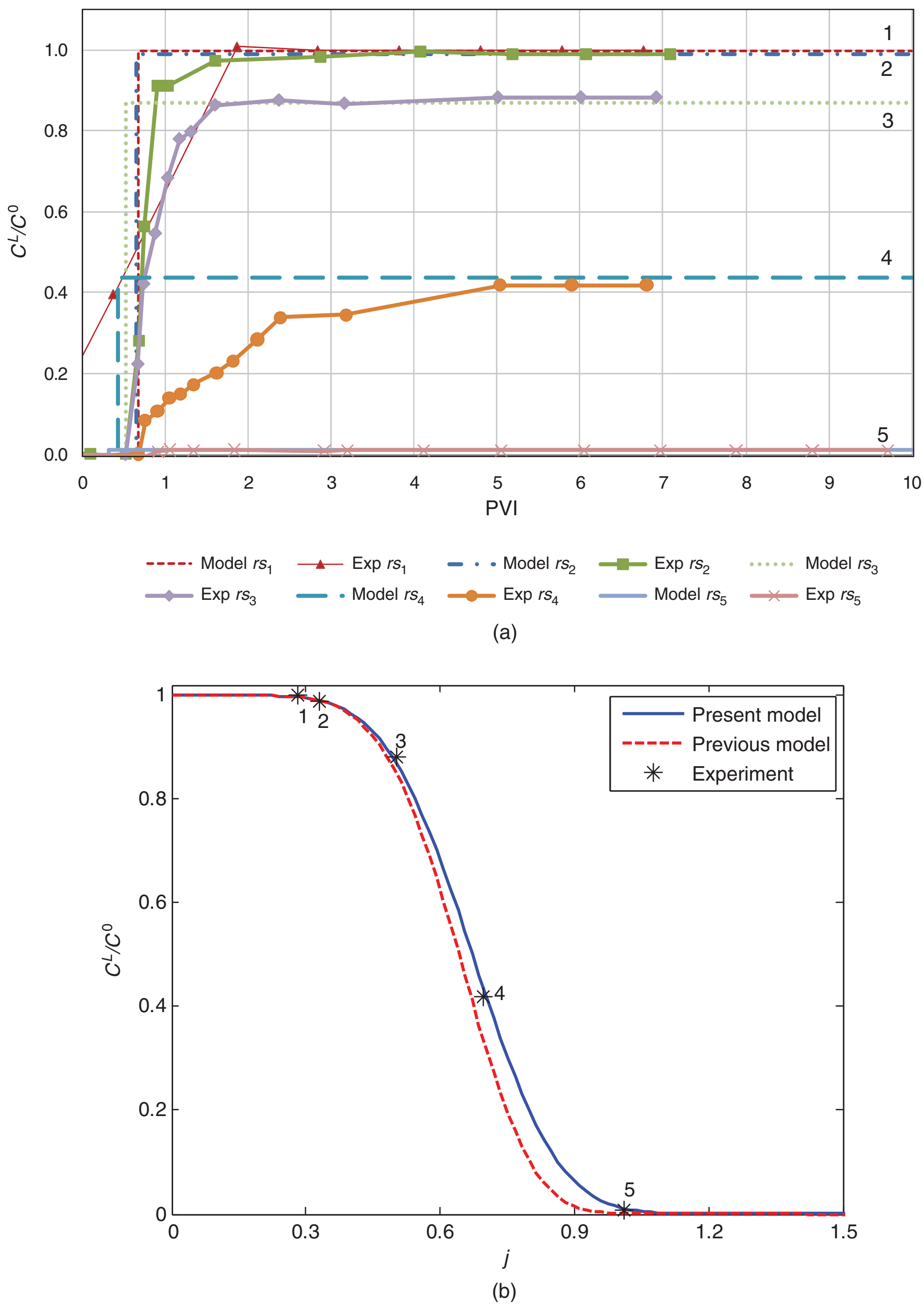

Fig. 5—Data treatment for PM1: (a) normalized breakthrough curves for five sized-particle suspensions and (b) normalized breakthrough concentrations vs. jamming ratio.

deviation σ_0 to the same degree (20%) yields a smaller change in the particle concentration compared with the variation of $\langle r_p \rangle$ in Fig. 7. In contrast, 20% variation of the interchamber distance l/L results in the smallest change in particle concentration (Fig. 9), which means it is the least sensitive parameter among the three. Table 3 provides the quantitative results measured by the values of residual R, which confirm that the mean pore radius is the most sensitive parameter and the interchamber distance is the least.

Comparison Between the Modified and Classical Deep-Bed Filtration Models. The classical deep-bed filtration model does not account for inlet concentration increase caused by redirecting all particles entering larger pores into the accessible fraction of large pores:

$$x = 0:\ C = C^0. \quad \text{(33)}$$

The capture probability is equal to the fractional flow through small pores (f_{ns}). Performing calculations similar to Eqs. 22 through 27 yields the following expression for the outlet concentration:

$$\frac{C^L(r_s)}{C^0(r_s)} = \exp\left[-\frac{f_{ns}(r_s)L}{f_a(r_s)l}\right]. \quad \text{(34)}$$

The classical deep-bed filtration model does not account for the outlet concentration decrease because of "dilution" of the flux, transported from PM by accessible flux in the overall water flux downstream of the core. Therefore, Eq. 34 is indeed the concentration measured at the core effluent. This model is currently used for colloidal-filtration-data treatment (Bailey et al. 2000; Buret et al. 2010).

Models (Eqs. 31 and 34) for the ratio of the inlet concentration to the outlet concentration differ by the term of multiplier $(1 - f_{ns})$

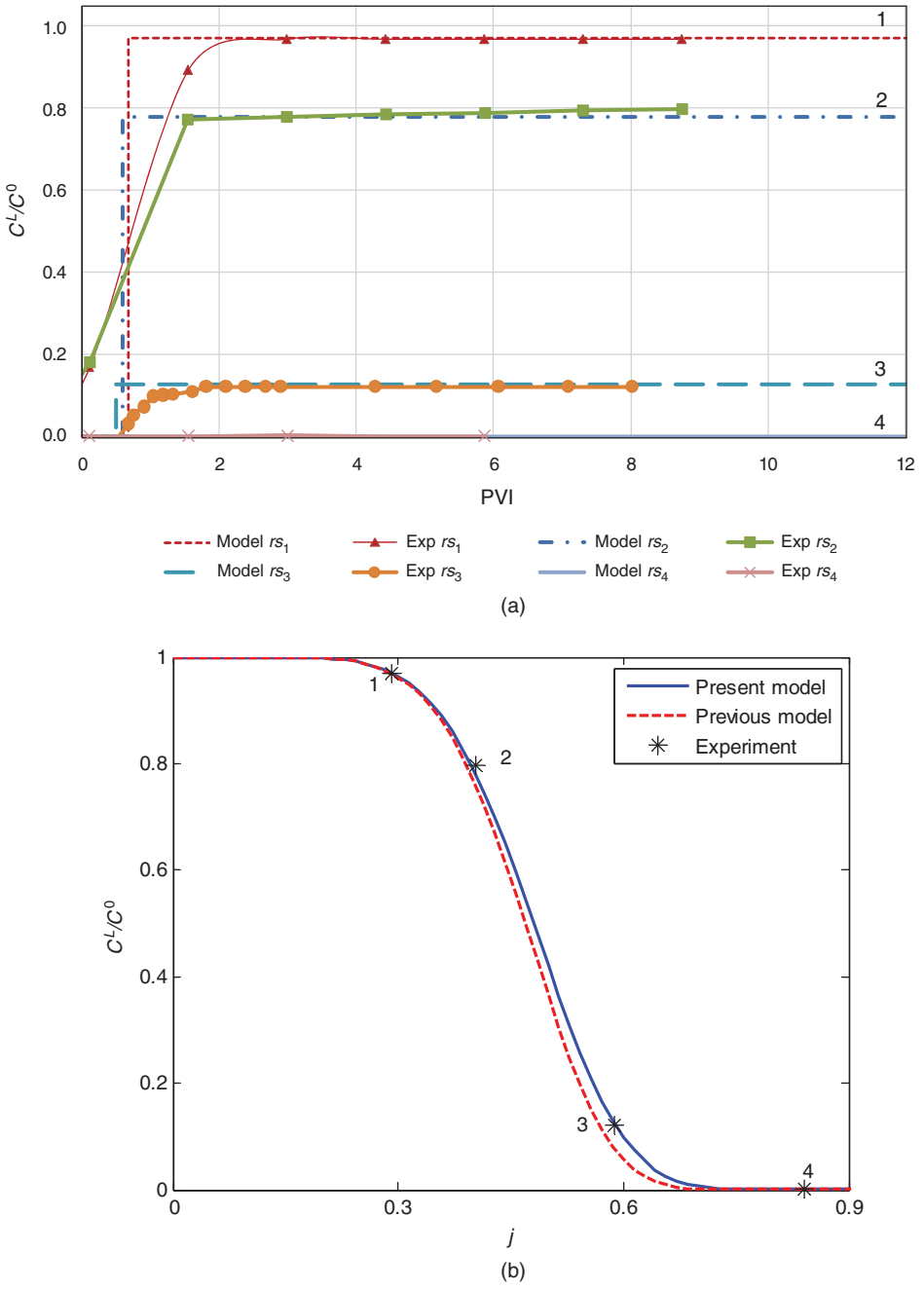

Fig. 6—Data treatment for PM2: (a) normalized breakthrough curves for four sized-particle suspensions and (b) normalized breakthrough concentrations vs. jamming ratio.

and the term under the exponent, $1/f_a$. Both terms equal unity for particles smaller than the minimum pore radius. Therefore, both the models (Eqs. 31 and 34) coincide for $r_s < r_{p\min}$. Both terms tend to zero for particles larger than the maximum pore radius. Therefore, for $j = 1$, the right-hand side of each formula tends to be zero (i.e., the models also coincide).

For intermediate particle sizes, taking off the term $(1 - f_{ns})$ from Eq. 31 increases the right-hand side. Yet, dividing the term f_a under the exponent yields the decrease of the right-hand side of Eq. 34. Therefore, it is impossible to claim a priori how the model modifications change the solution. Plots in Figs. 5b and 7b show that the deviation between the two models can be expected for particles with intermediate values of jamming ratio.

Figs. 5b and 7b also show the experimental points of the normalized outlet concentrations for continuous short-term injections of particles with different sizes (star points) and the curves $C^L/C^0(j)$, as obtained from the modified model (Eq. 31), by tuning the laboratory test data. The dashed curve is obtained from the model (Eq. 34). As it is shown, the modification of the inlet and outlet boundary conditions and accounting for fractional flow by means of accessible porous space in the particle-capture term can change the prediction of the curve $C^L/C^0(j)$ significantly.

The normalized concentrations of suspended particles along the core for small- and large-sized colloids are shown in **Figs. 10a and 10b,** respectively. The blue continuous curves are generated from the present model (Eq. 31), while the red dashed curves are from the previous model (Eq. 34). It is clear that the modified model predicts the concentration jump-up at the inlet and jump-down at the outlet, while the previous model does not. Furthermore, the concentration curve is almost linear for small-sized particles because of the small value of f_{ns}. For large particles, the exponential function takes effect, and the concentration decreases nonlinearly along the distance. Finally, both models result in almost the same outlet concentration for small-sized particles ($C^L/C^0 = 0.997$ for $r_s = 0.866$ μm in Fig. 10a), but differ for large particles ($r_s = 2.179$ μm in Fig. 10b); the modified model leads to

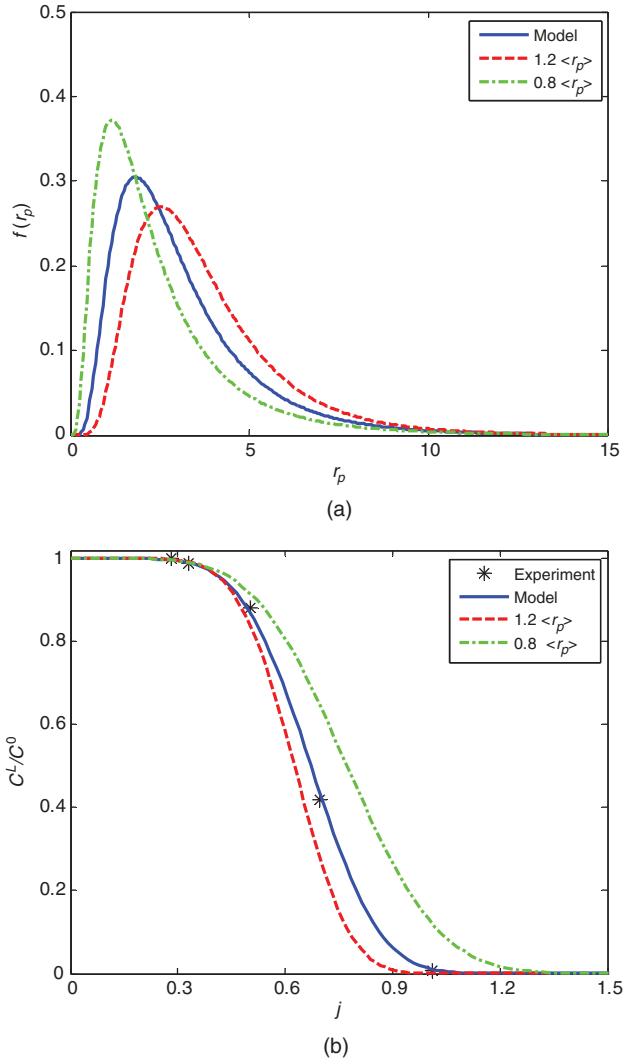

Fig. 7—Sensitivity of the breakthrough concentration with regard to mean pore-size variation: (a) PSD curves and (b) normalized breakthrough concentrations vs. jamming ratio.

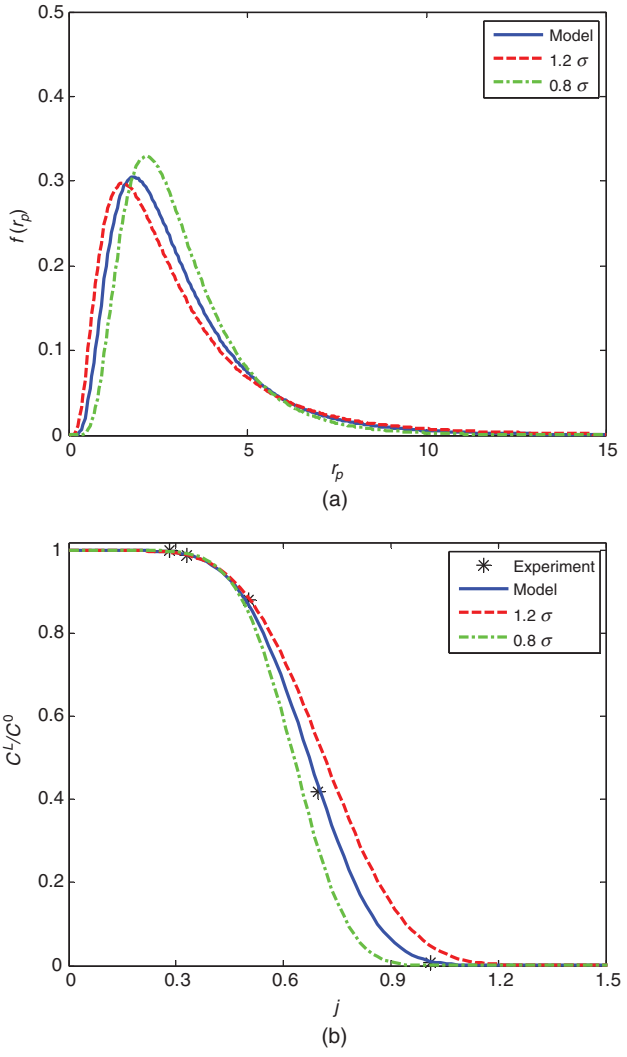

Fig. 8—Sensitivity of the breakthrough concentration with regard to standard deviation of pore sizes: (a) PSD curves and (b) normalized breakthrough concentrations vs. jamming ratio.

$C^L/C^0 = 0.44$, and the previous model results in $C^L/C^0 = 0.34$. This can also be observed in Fig. 5b.

Estimates of the Penetration Depth. Let us estimate the penetration depth of particles injected into the vertical openhole well.

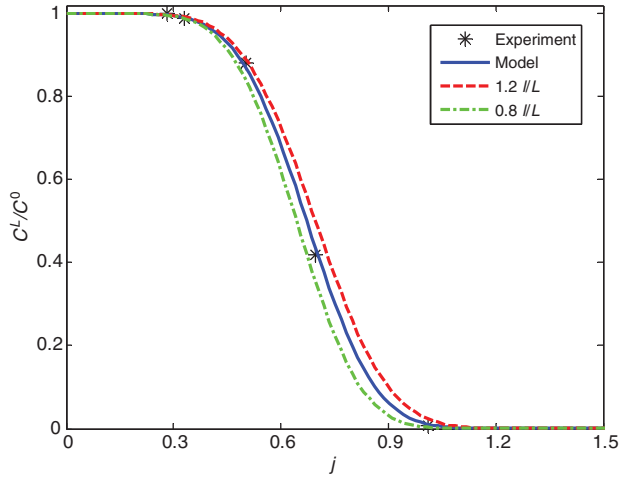

Fig. 9—Sensitivity of the breakthrough concentration with regard to the interchamber distance.

The penetration depth is an average of the current radius r in the penetrated zone, with weight equal to the concentration $C(r,t)$. Repeating the calculations as performed in Herzig et al. (1970) and Nunes et al. (2010) for the classical solution (Eq. 34) and using the modified solution (Eq. 31) for the axisymmetric flow, we obtain the following formula:

$$\langle r\rangle(r_s) = \frac{l}{f_a f_{ns}(r_s)}. \quad \ldots\ldots\ldots\ldots\ldots\ldots\ldots\ldots\ldots\ldots (35)$$

Fig. 11 presents the penetration depths of injected particles as a function of the particle/pore-jamming ratio. The calculations have been performed using the PSDs obtained from the suspension-injection tests with PM1 and PM2. The continuous curves correspond to the modified model (Eq. 31), while the dashed

TABLE 3—SENSITIVITY ANALYSIS FOR THE THREE PARAMETERS IN THE MODEL

Residual R for Three Cases	$\frac{\langle r_p\rangle}{\langle r_p\rangle_1}$	$\frac{\langle \sigma_0\rangle}{\langle \sigma_0\rangle_1}$	$\frac{\langle l/L\rangle}{\langle l/L\rangle_1}$
1.0	1.35×10^{-2}	1.35×10^{-2}	1.35×10^{-2}
1.2	6.51×10^{-2}	3.93×10^{-2}	2.69×10^{-2}
0.8	4.75×10^{-2}	3.57×10^{-2}	2.29×10^{-2}

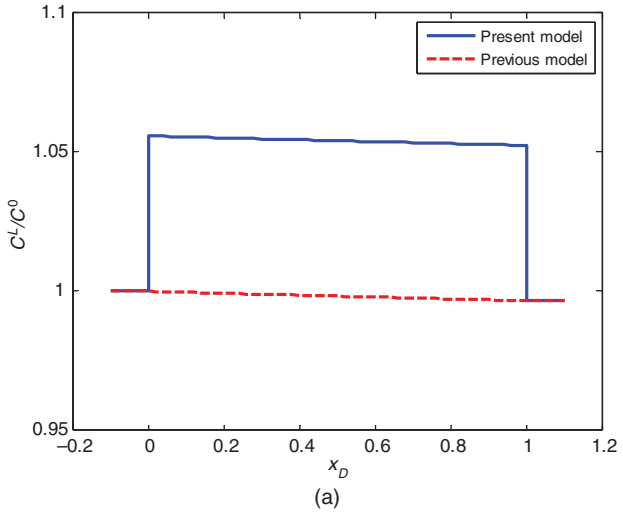

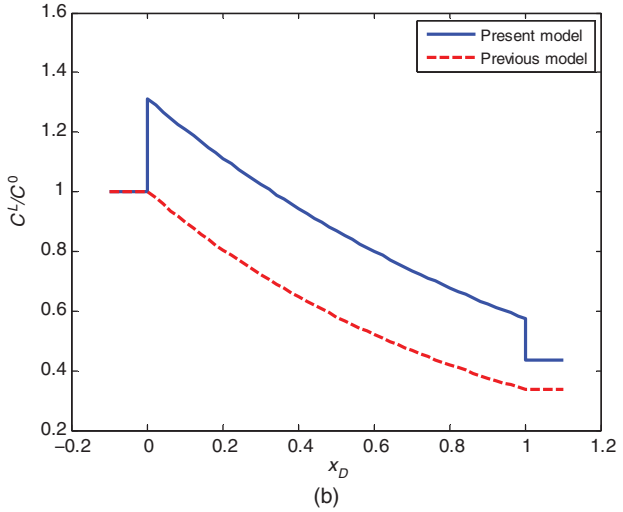

Fig. 10—Suspended concentration along the core: (a) r_{s1} = 0.866 μm and (b) r_{s4} = 2.179 μm.

curves show the results for the classical solution (Eq. 34). The experimental points lie on the continuous curves. The greater the particle size, the lesser the penetration depth. Because the mean pore-throat size is proportional to the square root of permeability, one concludes from Fig. 11 that the greater the permeability, the longer the mean particle penetration into the reservoir.

These data may be useful for particle sizing in drilling fluid (Bailey et al. 2000), for interpretation of logging data in drilling-fluid invasion into layer-cake formations (Tiab and Donaldson 2004), and for filtering of injected water (Pang and Sharma 1997). The results allow estimation of the extent of the formation-damage zone for design of well acidizing or reperforation.

Discussions

Even though the validation of the developed basic model and the analytical solution is successful, more-comprehensive research is needed to improve the model and the solution before recommendation for practical applications in petroleum technologies. Several potential improvements are discussed in this section.

The PM in the proposed analytical model is represented by a set of parallel capillaries intercalated by mixing chambers. However, it represents a simplified description of the pore-space geometry. More-sophisticated numerical network models or analytical percolation and effective media models would describe the topology of the pore network better.

The analytical model is developed under the assumption of low-retention filtration. It is a first-order asymptotic expansion of the solution with respect to the small parameter of retained particle concentration. In the present study, the ratio of the total number of retained particles to the vacant pores is kept below 0.1 throughout the tests to ensure that the conditions of particle capture, including the capture probability, remain the same during the overall injection period. The assumption of low-retention filtration is fulfilled during the injection process in the experiment. However, the maximum injection time is confined by this low-retention feature. Derivation of higher-order asymptotic expansions may describe the longer-term process with higher retention concentration. Another possible improvement is the numerical solution of the population-balance equations (Eqs. 18 through 21) for long-term injection processes.

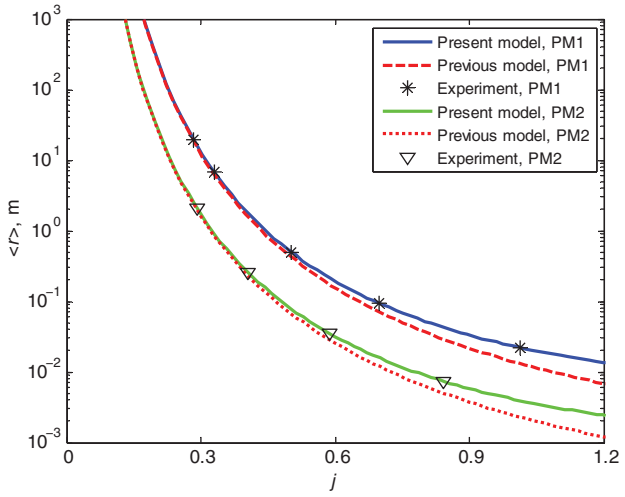

Fig. 11—Particle-penetration length vs. jamming ratio.

The effect of the inlet concentration increase is almost compensated by the effluent accessible flux dissolution in the overall water flux downstream of the porous column (Fig. 10b), which leads to a relatively small deviation between the concentration profiles, as obtained by the modified and previous models under the low-retention conditions. The situation may change for high-retention concentrations, in which the fractional flows are alternated at the inlet much more than at the effluent. Another case of large deviations between the modified and previous models is a colloidal pulse injection of large particles, in which the introduction of a small f_a term in the right-hand side of Eq. 19 results in significantly lower particle retention if compared with the previous model in which the fractional flow for accessible flux was not accounted for.

The derived mathematical model (Eqs. 18 though 21) describes suspension flow in PM with complex pore-space geometry. Two characteristic features of the flow in natural rocks are incorporated in the model:

- Independent flow of particles in larger pores
- Particle capture in capillary junctions in which the independent fluxes mix

The first feature is described by the particle flow in parallel capillary bundles between the mixing chambers. The mixing occurs in chambers; the capture takes place at the chamber exit after the mixing, describing the second feature. Separation of the two features allows derivation of the closed system of equations (Eqs. 18 and 19), while the general suspension flow in PM is described by network modeling (Sharma and Yortsos 1987a,b,c). Characterization of real reservoir rock using the population-balance model (Eqs. 18 and 19) includes determination of the initial PSD $H(r_p,x,0)$ and the interchamber distance l.

In this paper, validation of the model has been achieved by comparison with laboratory tests on the spherical particle suspensions through the glass-bead-packed porous column. The narrow PSD was achieved in the present study. Further validation must be performed for PM with larger variance coefficient for grain sizes. The next step must include colloid injections into natural reservoir cores.

Additional validation of the proposed model can be performed by measuring the retention profile (see Ali et al. 2009; Saraf et al. 2010). Yet, the experimental technique involving a computer-tomography (CT) scanner becomes much more complex than that used in the presented study. Also, only the bulk of the deposit can be determined by CT; different-sized particles in the retained volume cannot be distinguished.

The optimization-based matching of the experimental results shows that the data points are tuned well by the predicted curve generated from the theoretical model. Good agreement on the breakthrough concentrations between the experimental data and analytical-modeling results has been observed. Nevertheless, the amount and the range of experimental data have been circumscribed by the quite limited sizes of colloidal particles and glass beads that are readily available on the market. Preferably, more data points are needed to improve the reliability of optimizing the three model parameters: the mean radius, the standard deviation, and the interchamber distance.

The proposed model assumes the triangular pore-throat shape only. However, there may exist some caverns that cannot be plugged by particles in the hexagonal mode for a given grain-size distribution. More-complex pore-throat shapes, formed by four or more grains, could be taken into account in a more advanced model.

The proposed model estimates the approximate size of the formation-damage zone, which is useful for drilling, logging, and water injection. It assists in interpretation of logging data on filtrate invasion into oil- or gas-bearing formations, in particle sizing in drilling fluids, and in the design of injection-water filtering. It is also useful for determining the perforation lengths and the amount of injected acid with well stimulation. More-rigorous calculations would involve the development of the model for the permeability reduction by the retained different-sized particles. Despite serious attempts in this area (Pang and Sharma 1997; Mojarad and Settari 2007, 2008), such a model is unavailable at this time.

Mathematical modeling of emulsion flow in PM adds the effects of drops deformation and span-off to the model for suspension flow of solid particles. It would allow describing injectivity decline during produced-water reinjection (Rousseau et al. 2008; Ali et al. 2009; Buret et al. 2010).

Conclusions

The proposed stochastic model for particle-size exclusion deep-bed filtration differs from the previous models in the following aspects:

1. Introduction of the post-inlet particle concentration: The relationship between the particle concentration in the injected suspension and that at the PM entrance reflects particle capture in smaller pores and their passage by means of the accessible fraction of larger pores.
2. Introduction of the preoutlet particle concentration: The relationship between the suspended particle concentration at the outlet and that in the produced suspension reflects the particles carried by the accessible flux in situ and dissolved by the overall flux downstream of the PM.
3. Accounting for the particle-capture rate proportional to the accessible suspension flux.

The presented model shows a good agreement with laboratory data. The previous population-balance model shows a greater deviation of the prediction curves from the experimental data than the proposed model.

The sensitivity analysis of the model with respect to mean pore radius, standard deviation, and interchamber distance shows that the mean pore radius $\langle r_p \rangle$ has the largest effect on the resulting particle concentration C^L/C^0, the effect of standard deviation σ_0 is smaller compared with that of the mean pore radius, and the interchamber distance l/L is the least sensitive parameter.

Several improvements to the experimental setup have been implemented in the present study: Sieving of glass beads in the ultrasonic bath results in a reduced bead-sieving time and more-reproducible particle-size distribution, and the application of a dual-syringe-pump system leads to continuous pulseless colloidal-suspension pumping.

Nomenclature

c = total concentration of suspended particles, m^{-3}
c^0 = injected concentration of suspended particles, m^{-3}
C = concentration distribution of suspended particles, m^{-4}
C^0 = inlet concentration distribution of suspended particles, m^{-4}
C^L = outlet concentration distribution of suspended particles, m^{-4}
f_a = accessible flow fraction
f_{nl} = inaccessible flow fraction in large pores
f_{ns} = inaccessible flow fraction in small pores
h = total concentration of pores, m^{-2}
H = concentration distribution of pores, m^{-3}
j = jamming ratio
k_1 = pore conductance, m^4
k_{1a} = accessible pore conductance, m^4
l = interchamber distance, m
L = length scale, m
N_g = number of packed grains
N_p = number of pores
p = fraction of vacant pores
q_1 = flow rate in a single pore, m^3/s
r_g = grain radius, m
r_p = pore radius, m
r_s = particle radius, m
R = residual value
s_1 = cross-sectional area of pore throat, m^2
t = time, seconds
U = total flux, m/s
V = column volume, m^3
x = coordinate, m
γ = flux reduction factor in a single pore
σ = total retained particle concentration, m^{-3}
σ_0 = standard deviation for PSD, m
Σ = retained particle concentration distribution, m^{-4}
ϕ = porosity
ϕ_a = accessible porosity
χ = area accessibility fraction

Acknowledgments

Special thanks are given to Y. Yortsos (University of Southern California), A. Shapiro (Technical University of Denmark), and P. Currie (Delft University of Technology) for long-time cooperation in suspension-flow studies. The authors are grateful to A. Zeinijahromi for calculation of DLVO forces; P. Chalk, N. Gooding, and S. Hutten for development of previous preliminary laboratory procedures; and S. Duhan, K. Le, and C. McLindin for carrying out the laboratory tests (Case 2). Financial support from the Australian Research Council (ARC) Discovery Project 1094299 and Santos Pty. Ltd. is also gratefully acknowledged.

References

Ali, M.A.J., Currie, P.K., and Salman, M.J. 2009. The Effect of Residual Oil on Deep-Bed Filtration of Particles in Injection Water. *SPE Prod & Oper* **24** (1): 117–123. SPE-107619-PA. http://dx.doi.org/10.2118/107619-PA.

Bachman, R.C., Harding, T.G., Settari, A. et al. 2003. Coupled Simulation of Reservoir Flow, Geomechanics, and Formation Plugging With Application to High-Rate Produced Water Reinjection. Presented at the SPE Reservoir Symposium, Houston, 3–5 February. SPE-79695-MS. http://dx.doi.org/10.2118/79695-MS.

Bailey, L., Boek, E.S., Jacques, S.D.M. et al. 2000. Particulate Invasion From Drilling Fluids. *SPE J.* **5** (4): 412–419. SPE-67853-PA. http://dx.doi.org/10.2118/67853-PA.

Bedrikovetsky, P.G. 2008. Upscaling of Stochastic Micro Model for Suspension Transport in Porous Media. *Transport Porous Media* **75** (3): 335–369. http://dx.doi.org/10.1007/s11242-008-9228-6.

Bird, R.B., Stewart, W.E., and Lightfoot, E.N. 2007. *Transport Phenomena*, second revised edition. New York: John Wiley & Sons Publishing.

Bradford, S.A., Kim, H.N., Haznedaroglu, B.Z. et al. 2009. Coupled Factors Influencing Concentration-Dependent Colloid Transport and Retention in Saturated Porous Media. *Environ. Sci. Technol.* **43** (18): 6996–7002. http://dx.doi.org/10.1021/es900840d.

Bradford, S.A., Torkzaban, S., and Simunek, J. 2011. Modeling colloid transport and retention in saturated porous media under unfavorable attachment conditions. *Water Resour. Res.* **47** (10): art. no. W10503.

Buret, S., Nabzar, L., and Jada, A. 2010. Water Quality and Well Injectivity: Do Residual Oil-in-Water Emulsions Matter? *SPE J.* **15** (2): 557–568. SPE-122060-PA. http://dx.doi.org/10.2118/122060-PA.

Chalk, P., Gooding, N., Hutten, S.J. et al. 2011. Laboratory and Theoretical Investigation of Size Exclusion Suspension Flow in Rocks. Presented at the SPE European Formation Damage Conference, Noordwijk, The Netherlands, 7–10 June. SPE-144219-MS. http://dx.doi.org/10.2118/144219-MS.

Chatterjee, R., Mitra, S.K., and Bhattacharjee, S. 2011. Particle deposition onto Janus and patchy spherical collectors. *Langmuir* **27** (14): 8787–8797.

Chauveteau, G., Nabzar, L., and Coste, J.-P. 1998. Physics and Modeling of Permeability Damage Induced by Particle Deposition. Presented at the SPE Formation Damage Control Conference, Lafayette, Louisiana, USA, 18–19 February. SPE-39463-MS. http://dx.doi.org/10.2118/39463-MS.

Chupin, O., Saiyouri, N., and Hicher, P.-Y. 2008. The effects of filtration on the injection of cement-based grouts in sand columns. *Transport Porous Media* **72** (2): 227–240. http://dx.doi.org/10.1007/s11242-007-9146-z.

Civan, F. 2007. *Reservoir Formation Damage: Fundamentals, Modeling, Assessment, and Mitigation*, second edition. Burlington, Massachusetts: Gulf Professional Publishing/Elsevier.

Civan, F. 2010. Non-isothermal Permeability Impairment by Fines Migration and Deposition in Porous Media including Dispersive Transport. *Transport Porous Media* **85** (1): 233–258. http://dx.doi.org/10.1007/s11242-010-9557-0.

Cortis, A. and Berkowitz, B. 2004. Anomalous Transport in "Classical" Soil and Sand Columns. *Soil Sci. Soc. Am. J.* **68** (5): 1539–1548. http://dx.doi.org/10.2136/sssaj2004.1539.

Ding, D.Y. 2010. Modeling Formation Damage for Flow Simulations at Reservoir Scale. *SPE J.* **15** (3): 737–750. SPE-121805-PA. http://dx.doi.org/10.2118/121805-PA.

Gitis, V., Rubinstein, I., Livshits, M. et al. 2010. Deep-bed filtration model with multistage deposition kinetics. *Chem. Eng. J.* **163** (1–2): 78–85. http://dx.doi.org/10.1016/j.cej.2010.07.044.

Herzig, J.P., Leclerc, D.M., and LeGoff, P. 1970. Flow of Suspensions through Porous Media—Application to Deep Filtration. *Ind. Eng. Chem. Fundam.* **62** (5): 8–35. http://dx.doi.org/10.1021/ie50725a003.

Khilar, K.C. and Fogler, H.S. 1998. *Migration of Fines in Porous Media*. Dordrecht, The Netherlands: Theory and Applications of Transport in Porous Media, Kluwer Academic Publishers.

Kuznar, Z.A. and Elimelech, M. 2007. Direct microscopic observation of particle deposition in porous media: Role of the secondary energy minimum. *Colloids Surf., A* **294** (1–3): 156–162. http://dx.doi.org/10.1016/j.colsurfa.2006.08.007.

Landau, L.D. and Lifshitz, E.M. 1980. *Statistical Physics*, third edition, trans. J.B. Sykes and M.J. Kearsley, Part 1, Vol. 5. Oxford, UK: Course in Theoretical Physics, Butterworth-Heinemann.

Lin, H.-K., Pryadko, L.P., Walker, S. et al. 2009. Attachment and detachment rate distributions in deep-bed filtration. *Physical Review E* **79** (4): 046321. http://dx.doi.org/10.1103/PhysRevE.79.046321.

Massoudieh, A. and Ginn, T.R. 2010. Colloid-Facilitated Contaminant Transport in Unsaturated Porous Media. In *Modelling of Pollutants in Complex Environmental Systems, Volume II*, G. Hanrahan, Part III, Chap. 8, 263–286. Hertfordshire, UK: Advanced Topics in Environmental Science, ILM Publications.

Mays, D.C. and Hunt, J.R. 2005. Hydrodynamic Aspects of Particle Clogging in Porous Media. *Environ. Sci. Technol.* **39** (2): 577–584. http://dx.doi.org/10.1021/es049367k.

Mojarad, R.S. and Settari, A. 2007. Coupled Numerical Modelling of Reservoir Flow with Formation Plugging. *J Can Pet Technol* **46** (3): 54–59. JCPT Paper No. 07-03-05. http://dx.doi.org/10.2118/07-03-05.

Mojarad, R.S. and Settari, A. 2008. Velocity-based Formation Damage Characterization Method for Produced Water Re-injection: Application on Masila Block Core Flood Tests. *Petroleum Science and Technology* **26** (7-8): 937–954. http://dx.doi.org/10.1080/10916460701825596.

Nabzar, L., Chauveteau, G., and Roque, C. 1996. A New Model for Formation Damage by Particle Retention. Presented at the SPE Formation Damage Control Conference, Lafayette, Louisiana, USA, 14–15 February. SPE-31119-MS. http://dx.doi.org/10.2118/31119-MS.

Noubactep, C. and Caré, S. 2010. Dimensioning metallic iron beds for efficient contaminant removal. *Chem. Eng. J.* **163** (3): 454–460. http://dx.doi.org/10.1016/j.cej.2010.07.051.

Nunes, M., Bedrikovetsky, P., Newbery, B. et al. 2010. Theoretical Definition of Formation Damage Zone With Applications to Well Stimulation. *J. Energy Resour. Technol.* **132** (3): 033101–7. http://dx.doi.org/10.1115/1.4001800.

Pang, S. and Sharma, M.M. 1997. A Model for Predicting Injectivity Decline in Water-Injection Wells. *SPE Form Eval* **12** (3): 194–201. SPE-28489-PA. http://dx.doi.org/10.2118/28489-PA.

Richards, T. and Neretnieks, I. 2010. Filtering of Clay Colloids in Bentonite Detritus Material. *Chem. Eng. Technol.* **33** (8): 1303–1310. http://dx.doi.org/10.1002/ceat.201000108.

Rousseau, D., Hadi, L., and Nabzar, L. 2008. Injectivity Decline From Produced-Water Reinjection: New Insights on In-Depth Particle-Deposition Mechanisms. *SPE Prod & Oper* **23** (4): 525–531. SPE-107666-PA. http://dx.doi.org/10.2118/107666-PA.

Saraf, A., de Zwart, A.H., Currie, P.K. et al. 2010. Analysis of the Effect of Residual Oil on Particle Trapping During Produced-Water Reinjection Using X-Ray Tomography. *SPE J.* **15** (4): 943–951. SPE-122137-PA. http://dx.doi.org/10.2118/122137-PA.

Schembre, J.M. and Kovscek, A.R. 2005. A mechanism of formation damage at elevated temperature. *J. Energy Resour. Technol.* **127** (3): 171–180.

Shapiro, A.A. and Bedrikovetsky, P.G. 2008. Elliptic random-walk equation for suspension and tracer transport in porous media. *Physica A* **387** (24): 5963–5978. http://dx.doi.org/10.1016/j.physa.2008.07.013.

Shapiro, A.A. and Bedrikovetsky, P.G. 2010. A stochastic theory for deep bed filtration accounting for dispersion and size distributions. *Physica A* **389** (13): 2473–2494. http://dx.doi.org/10.1016/j.physa.2010.02.049.

Sharma, M.M. and Yortsos, Y.C. 1987a. Transport of particulate suspensions in porous media: Model formulation. *AIChE J.* **33** (10): 1636–1643. http://dx.doi.org/10.1002/aic.690331007.

Sharma, M.M. and Yortsos, Y.C. 1987b. A network model for deep bed filtration processes. *AIChE J.* **33** (10): 1644–1653. http://dx.doi.org/10.1002/aic.690331008.

Sharma, M.M. and Yortsos, Y.C. 1987c. Fines migration in porous media. *AIChE J.* **33** (10): 1654–1662. http://dx.doi.org/10.1002/aic.690331009.

Takahashi, S. and Kovscek, A.R. 2010. Wettability estimation of low-permeability, siliceous shale using surface forces. *J. Pet. Sci. Eng.* **75** (1–2): 33–43. http://dx.doi.org/10.1016/j.petrol.2010.10.008.

Taylor, B.N. and Kuyatt, C.E. 1994. Guidelines for Evaluating and Expressing the Uncertainty of NIST Measurement Results. NIST Technical Note 1297, 1994 Edition (Supersedes NIST Technical Note 1297, January 1993), United States Department of Commerce Technology Administration, National Institute of Standards and Technology (NIST), Gaithersburg, Maryland (September 1994), http://physics.nist.gov/Pubs/guidelines/TN1297/tn1297s.pdf.

Tiab, D. and Donaldson, E.C. 2004. *Petrophysics: Theory and Practices of Measuring Reservoir Rock and Fluid Transport Properties*, second edition. Oxford, UK: Gulf Professional Publishing.

Torkzaban, S., Kim, H.N., Simunek, J. et al. 2010. Hysteresis of colloid retention and release in saturated porous media during transients in solution chemistry. *Environ. Sci. Technol.* **44** (5): 1662–1669

Tufenkji, N. 2007. Colloid and Microbe Migration in Granular Environments: A Discussion of Modelling Methods. In *Colloidal Transport in Porous Media*, ed. F.H. Frimmel, F. von-der-Kammer, and H.-C. Flemming, Chap. 5, 119–137. Berlin, Germany: Springer-Verlag.

Tufenkji, N. and Elimelech, M. 2004. Deviation from the Classical Colloid Filtration Theory in the Presence of Repulsive DLVO Interactions. *Langmuir* **20** (25): 10818–10828. http://dx.doi.org/10.1021/la0486638.

Tufenkji, N. and Elimelech, M. 2005. Reply to Comment on Breakdown of Colloid Filtration Theory: Role of the Secondary Energy Minimum

and Surface Charge Heterogeneities. *Langmuir* **21** (23): 10896–10897. http://dx.doi.org/10.1021/la051621e.

Zhou, J., Zheng, X., Flury, M. et al. 2009. Permeability changes during remediation of an aquifer affected by sea-water intrusion: A laboratory column study. *J. Hydrol.* **376** (3–4): 557–566. http://dx.doi.org/10.1016/j.jhydrol.2009.07.067.

Zhenjiang You is a research fellow in the Australian School of Petroleum at the University of Adelaide. Research interests include modeling of suspension transport in PM; flow distribution within gas and oil wells; and formation damage in geothermal reservoirs. You holds a BEng degree in engineering mechanics and a PhD degree in fluid mechanics, both from Zhejiang University.

Alexander Badalyan is an ARC senior research associate in the Australian School of Petroleum at the University of Adelaide. His research interests include, but are not limited to, suspension flow in PM, characterization of porous solids by nanometric gas adsorption, and thermophysical properties of fluids. Badalyan holds one Australian patent and is the author/coauthor of several international and SPE journal and conference papers. He holds a bachelor's degree in automatic control from Grozny Petroleum Institute and a PhD degree in theoretical fundamentals of heat engineering (thermophysical properties of fluids) from Azerbaijan Petroleum and Chemistry Institute.

Pavel Bedrikovetsky is a professor in the Australian School of Petroleum at the University of Adelaide. He is also a senior staff consultant to Petrobras in the areas of formation damage, waterflooding, and improved oil recovery. During 1991–94, Bedrikovetsky was a visiting professor at Delft University of Technology and at Imperial College of Science and Technology. His main research interests include formation damage, suspension/colloid transport in PM, and mathematical modeling of well stimulation and exploitation of unconventional energy resources. Bedrikovetsky is the author of two books on reservoir engineering and 150 technical papers published in international and SPE journals. He holds BEng and MSc degrees in applied mathematics, a PhD degree in fluid mechanics, and a DSc degree in reservoir engineering, all from Moscow Gubkin Petroleum University. Bedrikovetsky served as section chairperson, short-course instructor, key speaker, and steering committee member at several SPE conferences, and he was a 2008–09 SPE Distinguished Lecturer.